Appl Phys B (2011) 103: 311–319
DOI 10.1007/s00340-010-4297-y

Applied Physics B
Lasers and Optics

Low-threshold singly-resonant continuous-wave optical parametric oscillator based on MgO-doped PPLN

I.-H. Bae · H.S. Moon · S. Zaske · C. Becher · S.K. Kim · S.-N. Park · D.-H. Lee

Received: 1 July 2010 / Revised version: 27 August 2010 / Published online: 20 November 2010

Abstract We present a 532 nm-pumped singly-resonant cw optical parametric oscillator based on MgO-doped PPLN with a minimum threshold pump power of 0.3 W. The OPO with a two-mirror standing-wave cavity is optimized by using a tunable diode laser on the path of the resonant signal beam. The maximum output power is 200 mW at an idler wavelength near 1330 nm at a pump power of 2 W. We report the degradation of the output power and beam characteristics at high pump power indicating a strong thermal lensing in the crystal. The continuous tuning range of the OPO is measured to be 800 MHz which is close to 90% of the free spectral range of the OPO cavity.

1 Introduction

Continuous-wave (cw) optical parametric oscillators (OPOs) are prominent coherent radiation sources especially in the infrared due to, above all, their excellent wavelength tunability. Since the first demonstration in 1968 [1], the development of cw OPOs is stimulated by the rapid technical progress of cw pump lasers and high-quality nonlinear materials. In particular, the application of quasi-phase matching (QPM) by using periodically poled nonlinear crystals made cw OPOs more useful and practical with the possibility of engineering the nonlinear materials for the desired interactions [2]. Various types of cw OPOs based on QPM are realized in the last two decades using periodically poled (PP) nonlinear crystals such as $LiNbO_3$ (LN), $LiTaO_3$ (LT), $KTiOPO_4$ (KTP), and $RbTiOAsO_4$ (RTA) pumped by solid-state lasers and diode lasers [3].

Recently, cw OPOs with new materials such as MgO-doped stoichiometric PPLT and MgO-doped PPLN for better resistance to photo-refractive damage are reported [4, 5]. An OPO converts the input pump wave into the signal and idler output waves at different wavelengths based on the phase-matched three-wave mixing in its nonlinear crystal placed in an optical cavity. Depending on how many of the three interacting waves are resonated by the cavity, the OPO can be classified to be singly resonant, doubly resonant, or triply resonant. Singly-resonant OPOs, in which only the signal or the idler wave is resonated, generally offer superior power and frequency stability, conversion efficiency, and tuning property compared to the other designs. They require, however, much more pump power to achieve the oscillation threshold [6].

The oscillation threshold of a singly-resonant OPO is dominantly determined by the parameters such as the nonlinearity and the length of the used crystal, the optical loss in the cavity, the pump wavelength, and the mode matching between the pump wave and the resonated wave [3]. The first demonstration of a singly-resonant cw OPO was reported in 1993, which utilized a KTP crystal inside a three-mirror standing-wave cavity [7]. Pumped at 532 nm, the oscillation threshold of this KTP OPO was achieved at a pump power of 1.4 W. Change of its cavity design to a four-mirror ring cavity, however, increased the threshold pump power to 4.3 W [8]. In 1996, the first cw quasi-phase-matched

I.-H. Bae · H.S. Moon (✉)
Department of Physics, Pusan National University, Busan 609-735, Rep. Korea
e-mail: hsmoon@pusan.ac.kr

S. Zaske · C. Becher
Fachrichtung 7.3 (Technische Physik), Universität des Saarlandes, 66123, Saarbrücken, Germany

S.K. Kim · S.-N. Park · D.-H. Lee (✉)
Division of Physical Metrology, Korea Research Institute of Standards and Science (KRISS), Daejeon 305-340, Rep. Korea
e-mail: dh.lee@kriss.re.kr

OPO was demonstrated based on bulk PPLN pumped at 1064 nm [9, 10]. The threshold pump power for a two-mirror standing-wave cavity and for a four-mirror ring cavity was 2.6 W and 3.6 W, respectively, for this infrared-pumped PPLN OPO. For a green-pumped cw singly-resonant OPO based on bulk PPLN, the threshold pump power was further reduced down to 1.2 W even in a ring-cavity design [11]. Singly-resonant OPOs based on MgO-doped PPLN and MgO-doped stoichiometric PPLT are reported to reduce the threshold pump power down to 0.5 W in a high-finesse cavity condition [12, 13]. Very recently, a threshold pump power of as low as 0.46 W is reported for a singly-resonant green-pumped OPO using a 50-mm long MgO-doped PPLN crystal and a 2% output coupling mirror in a four-mirror ring cavity [14].

In this paper, we present a singly-resonant cw OPO with a minimum threshold pump power of 0.3 W, which is close to the theoretical optimum for the given experimental parameters. The OPO is based on a 40-mm long MgO-doped PPLN placed in a two-mirror standing-wave cavity for the signal wave with a 2% output coupling mirror. The two-mirror standing-wave cavity design in general provides advantages of simple setup and lower loss compared to the ring-cavity design. But the tuning characteristics of the standing-wave cavity are known to be inferior to the ring cavity due to residual etalon effects inside the cavity [8]. Note, however, that the optimization method for the low oscillation threshold operation, which we will minutely describe in the next chapter, can be applied not only for the two-mirror cavity but also for the ring-cavity OPOs.

Pumped at 532 nm, the tuning range in which the OPO operates with a low oscillation threshold below 0.5 W was from 800 nm to 890 nm and from 1330 nm to 1600 nm for the signal and idler wavelength, respectively. The output power, however, was not correlated to the oscillation threshold, but strongly dependent upon pump power and cavity alignment condition. By observing the degradation of output power and spatial beam quality with the increasing pump power, we confirmed that strong thermal lensing in the MgO-doped PPLN crystal limits the performance of the OPO [15, 16]. The maximum output power at a pump power of 2 W was approximately 100 mW and 200 mW at the signal and idler wavelength of 885 nm and 1333 nm, respectively. The range of continuous frequency tuning by scanning the cavity length without any frequency-selective element inside the cavity is measured to be 800 MHz that is close to 90% of the free spectral range of the cavity of 900 MHz.

2 Experimental setup and optimization

Figure 1 schematically shows the experimental setup of the cw singly-resonant OPO. As the pump laser, a diode-pumped solid-state (DPSS) laser (Model Verdi, Coherent, Santa Clara, California) is used, which provides a radiant power of up to 5 W in a single-frequency single-spatial-mode beam at a wavelength of 532 nm. The collimated pump beam is, after passing through a Faraday isolator, focused by a plano-convex lens (F1) with a focal length of 150 mm onto the center of the OPO cavity for spatial-mode matching. The OPO cavity is a linear standing-wave optical cavity consisting of two mirrors M1 and M2 with the nonlinear crystal at its center.

The nonlinear crystal is a congruent-melt $LiNbO_3$ with 5 mol% MgO doping in a dimension of 40 mm $\times$ 8 mm $\times$ 0.5 mm, which is periodically poled for four different poling periods $\Lambda = (7.2, 7.4, 7.6, 7.8)$ μm (HC Photonics, Hsinchu, Taiwan). The two facets of the crystal are optically flat polished without wedging and coated for anti-reflection at wavelengths of 532 nm, 850 nm, and 1450 nm. The crystal is mounted on a kinematic stage for alignment and its temperature is stabilized and controlled within ± 0.05°C. Cavity mirrors M1 and M2 are both plano-concave types with a radius of curvature of 50 mm. The plane sides of both mirrors are anti-reflection coated at the same wavelengths as the crystal facets. The concave side of M1 is coated for high reflectance ($R > 99\%$ at the signal wavelength and high trans-

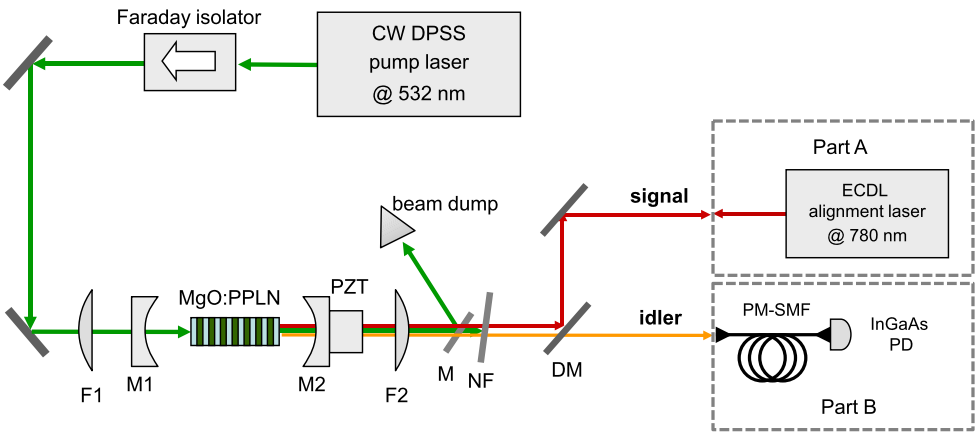

Fig. 1 Schematic diagram of the low-threshold singly-resonant cw OPO based on MgO-doped PPLN. Part A is attached for the initial alignment of the OPO cavity. Part B is attached to monitor the continuous-tuning property. The abbreviations are defined in the text

mittance ($T > 90\%$) at the pump and idler wavelengths; the M2 is coated for 2% transmission at the signal wavelength and high transmission at the pump and idler wavelengths. M1 and M2 are placed approximately 120 mm apart to build a near-concentric resonator [17] only for the signal wave. The cavity length can be varied by a cylinder-type piezoelectric transducer (PZT) attached to the reverse of M2. The output beams from the OPO cavity are collimated by another plano-convex lens (F2) with a focal length of 150 mm. The pump beam transmitted through the OPO cavity is separated from the signal and idler beams by using a mirror (M) that is highly reflective only at 532 nm. The residual pump beam is blocked using a notch filter (NF) for 532 nm. Subsequently, the signal beam is separated from the idler beam by a dichroic beam-splitting mirror (DM).

For the alignment of the OPO cavity, we used a grating-stabilized external-cavity diode laser (ECDL) in Littrow configuration (Model DL100, Toptica, Munich, Germany) emitting single-frequency radiation at 780 nm. In the initial stage of the setup, before the cavity mirrors are installed, the alignment ECDL is positioned at the signal output port of the OPO, as shown in Part A of Fig. 1, and its beam is aligned so that the pump beam and the ECDL beam completely overlap in free space but propagate in the opposite directions. Then, the cavity mirrors and the crystal are placed along the optical axis defined by the two overlapped beams so that the OPO cavity builds now a Fabry–Pérot interferometer for the ECDL beam. By periodically varying the cavity length via the PZT behind the mirror M2 and recording the transmitted power of the ECDL beam using a photo diode behind the mirror M1, we obtain the spectrum of the ECDL beam, which approaches a single longitudinal mode as the cavity alignment and the mode matching of the ECDL beam is optimized.

Figure 2 shows spectra of the ECDL measured before (a) and after (b) optimization of the OPO cavity. Note that the time axis of Fig. 2 can be scaled to frequency when we know the exact value of the free spectral range (FSR) of the cavity. In the spectrum (a) of Fig. 2, one sees two sets of the transversal mode peaks (α, β, γ) and (α', β', γ') which are separated by a FSR. From the position and the behavior to the cavity alignment, we identify that the peaks α and α' correspond to the fundamental TEM_{00} modes, the peaks β and β' to a superposition of the TEM_{01} and TEM_{10} modes, and the peaks γ and γ' a superposition of the TEM_{02} and TEM_{20} modes [17]. When the cavity is optimally aligned as in the spectrum (b) of Fig. 2, the high-order transversal mode peaks (β, γ) and (β', γ') disappear while the fundamental mode peaks α and α' become stronger. We observe, however, the additional peaks δ and δ' in the spectrum (b) of Fig. 2, which arise at the positions near the peaks γ and γ'. These peaks correspond to the high-order transversal modes excited by a non-perfect spatial matching of the ECDL beam

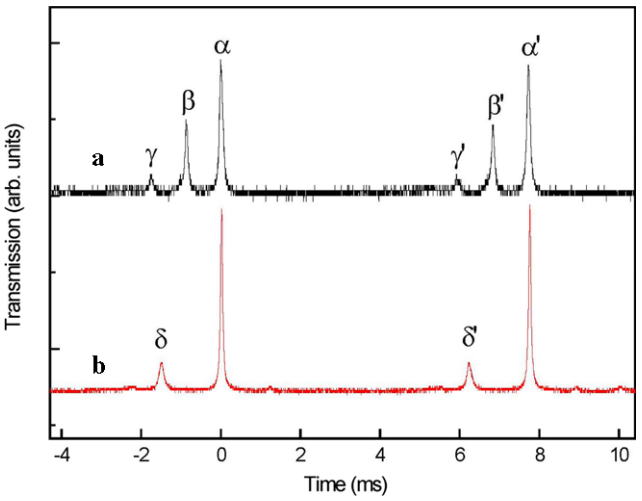

Fig. 2 Fabry–Pérot spectrum of the alignment ECDL beam measured through the OPO cavity (**a**) before and (**b**) after optimization. The transmitted power of the ECDL beam is measured using a photodiode and recorded as a function of time while the cavity length is periodically scanned. The *Greek characters* denote the different resonant peaks

mode to the cavity fundamental mode, which cannot be removed only from optimization of the cavity alignment. We also see several other peaks in the spectrum (b) of Fig. 2, which originate from the longitudinal mode spectrum of the ECDL beam. The ECDL used in this experiment contains a laser diode without anti-reflection coating on the exit facet and, therefore, has a poor side mode suppression.

A measurement of the spectrum of the alignment ECDL as shown in Fig. 2 is useful not only to optimize the OPO cavity alignment with high sensitivity, but also to determine the confocal parameter of the cavity for the resonant signal wave. Knowing the confocal parameter of the resonant cavity is important to optimize the beam focusing and the mode-overlap between the pump beam and the spatial mode of the output waves, which critically influence the parametric gain and the oscillation threshold [18]. We note that the optimization of the beam focusing is more simple for a pump-resonant OPO because the confocal parameter can be determined directly from a transmission spectrum of the pump wave through the OPO cavity [19]. In the case of a singly-resonant OPO, however, measurement of a spectrum such as Fig. 2 by using an extra laser resonant to the OPO cavity is recommended to determine the confocal parameter more accurately. We describe in the following how we determine the confocal parameter from the measurement of Fig. 2.

For a symmetric cavity consisting of two concave mirrors with radius of curvature r, the confocal parameter b can be calculated from the cavity length L by the following equation [17]:

$$b = \sqrt{2L(2r - L)}. \quad (1)$$

The cavity length L can be measured either from a direct measurement of the geometric distance between the two mirrors or from a measurement of the spatial-mode spectrum of the cavity, such as Fig. 2, according to the equation

$$\frac{\Delta\nu}{\mathrm{FSR}} = \frac{1}{\pi}\left|\arccos\left(1-\frac{L}{r}\right)\right|, \tag{2}$$

where FSR denotes the free spectral range of the cavity and $\Delta\nu$ the frequency distance between the fundamental mode and the first adjacent transversal mode. If the cavity, however, contains a crystal with a length L_c and a refractive index n as shown in Fig. 1, we should consider the refraction according to Snell's law by replacing the length L_c by L_c/n inside the crystal [17]. Therefore, for the OPO cavity with the geometric length of L_{geo} including the crystal, we should replace the cavity length L in (1) and (2) by the effective cavity length L_{eff} defined as

$$L_{\mathrm{eff}} = L_{\mathrm{geo}} - L_c + L_c/n. \tag{3}$$

On the other hand, the optical length L_{opt} of the cavity, which is related to the FSR of the cavity according to $\mathrm{FSR} = c/2L_{\mathrm{opt}}$, should be changed by the crystal to

$$L_{\mathrm{opt}} = L_{\mathrm{geo}} - L_c + nL_c. \tag{4}$$

In the measured spectrum (a) in Fig. 2, the ratio $\Delta\nu/\mathrm{FSR}$ in (2) corresponds to the ratio of the distance between, e.g., the peaks α and β to the distance between the peaks α and α', from which we can calculate the effective cavity length $L_{\mathrm{eff}} = 96.7$ mm and, with (1), the confocal parameter $b = 25.3$ mm. For comparison, the effective cavity length can be also calculated based on (3) from the measured geometric length $L_{\mathrm{geo}} = 119$ mm, the crystal length $L_c = 40$ mm, and the reference data of the refractive index $n = 2.17$ at a wavelength near 800 nm [20]. The result based on (3) is then $L_{\mathrm{eff}} = 97.4$ mm, which is approximately 7% larger than the result based on the measurement of Fig. 2. However, the accuracy of the data used for (3) is low due to, e.g., the limited accuracy of the measurement of the geometric length L_{geo} in practice. Consequently, we used the result $L_{\mathrm{eff}} = 96.7$ mm based on the measurement of Fig. 2 with (2) as the reference to determine the confocal parameter and also other parameters of the cavity: $b = 25.3$ mm from (1), $L_{\mathrm{geo}} = 118.3$ mm from (3), and $L_{\mathrm{opt}} = 165.1$ mm from (4).

For the above parameters determined from Fig. 2, the focusing parameter defined as $\xi = L_c/b$ is 1.58, which is much smaller than the theoretical optimal value of 2.8 [18] and also smaller than the empirical optimal value of 2.0 [19]. Therefore, in order to have an optimal operation of the OPO with a low oscillation threshold, we adjusted the cavity length until the effective cavity length and the confocal parameter are close to the values $L_{\mathrm{eff}} = 98$ mm and $b = 19.8$ mm, respectively, resulting in a focusing parameter of $\xi = 2.02$. The corresponding geometric and optical lengths of the cavity are $L_{\mathrm{geo}} = 119.6$ mm and $L_{\mathrm{opt}} = 166.4$ mm, respectively. The free spectral range of the cavity is then FSR = 901 MHz at a signal wavelength near 800 nm.

The next step of the optimization is the mode matching of the non-resonant pump beam to the resonant signal cavity fundamental mode. In practice, this is achieved by focusing the pump beam to a beam waist matched to that of the cavity mode. The radius w_0 of the beam waist of the cavity can be calculated from the confocal parameter according to the relation [17]

$$b = \frac{2\pi}{\lambda}w_0^2, \tag{5}$$

where λ denotes the wavelength of the resonant wave in air. For $b = 19.8$ mm and $\lambda = 800$ nm, we obtain $w_0 = 50.2$ μm for the OPO cavity. The pump beam waist w_p can be estimated from the diameter of the collimated pump beam D, the focal length of the mode-matching lens (F1 in Fig. 1) f, and the pump wavelength λ_p according to the following relation for a Gaussian beam [21]:

$$w_p \simeq \frac{f\lambda_p}{D}. \tag{6}$$

We measured the diameter of the collimated pump beam using a scanning-slit beam profiler (model BP109-UV, ThorLabs) at the position of the focusing lens F1 in Fig. 1 as $D = 1.9$ mm. For the selected lens with $f = 150$ mm, we obtain for the pump beam waist $w_p = 42$ μm. Although this value is smaller than the target value of 50.2 μm, we confirm later from the achieved performance of the OPO that the mode matching can be regarded as optimized within the tolerance of the parameter estimation.

Once the alignment of the cavity mirrors, the focusing parameter of the cavity, and the mode matching of the pump beam to the cavity were optimized as discussed above, we could start the OPO only by slightly adjusting the direction of the pump beam at a moderate pump power above 1 W. Further optimization of the OPO performance is accomplished by maximizing the OPO output power at a pump power that is now adjusted slightly above the oscillation threshold. By repeating this optimization procedure near threshold, we could finally reach an OPO operating at its minimum threshold condition. The characteristics and performance of the singly-resonant OPO optimized for the minimum oscillation threshold are presented in the following sections.

3 Wavelength tuning via temperature

Figure 3 shows the output wavelengths of the singly-resonant cw OPO measured with a double-grating optical

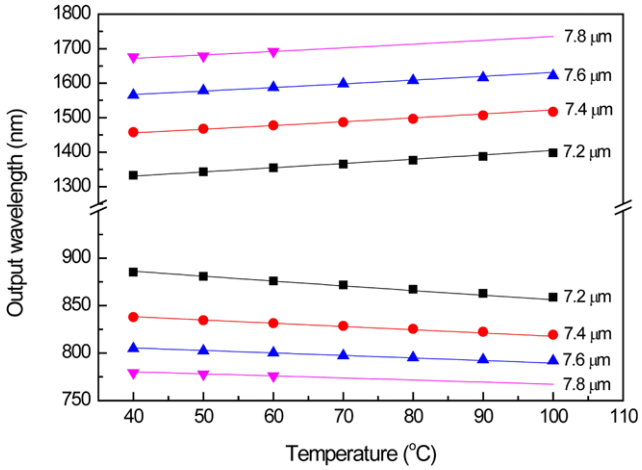

Fig. 3 Measured signal and idler output wavelengths of the singly-resonant cw OPO based on MgO-doped PPLN as a function of crystal temperature for different poling periods from 7.2 μm to 7.8 μm (symbols). The *solid lines* represent the theoretical prediction calculated from the dispersion relations for a 5 mol% MgO-doped congruent PPLN crystal, which is plotted with a temperature offset of 10°C

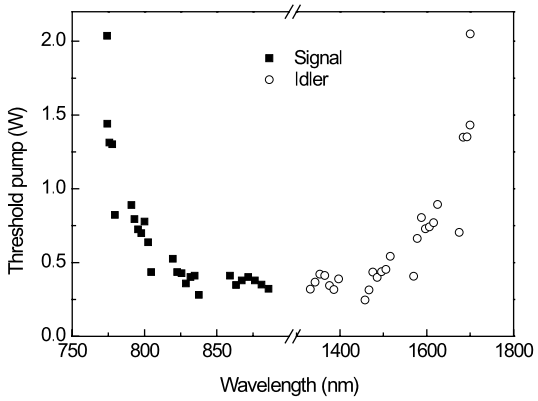

Fig. 4 Measured threshold pump power of the singly-resonant cw OPO as a function of output wavelength

spectrum analyzer (Model 86142B, Agilent Technologies, Santa Clara, California) plotted as a function of the crystal temperature for different poling periods (different symbols). The poling periods are selected by transversally translating the crystal with respect to the beam axis of the cavity. Adjusting the poling period from 7.2 μm to 7.8 μm and the crystal temperature from 40°C to 100°C allows the OPO to cover a range from 770 nm to 890 nm and from 1330 nm to 1680 nm for signal and idler, respectively. This tuning range is limited mainly by the spectral range of the highly reflective coatings on the cavity mirrors.

The output wavelengths of the cw OPO for a given poling period and crystal temperature can be calculated from the temperature-dependent dispersion relations (Sellmeier equations) and the quasi-phase-matching condition [20]. We calculated the expected phase-matching wavelengths based on the Sellmeier equations for a 5 mol% MgO-doped congruent PPLN crystal published by Gayer et al. in 2008 [22]. The calculated values are plotted in Fig. 3 as solid lines with a temperature offset of 10°C, i.e. a value calculated at a temperature of T is plotted in Fig. 3 at a temperature of $T + 10$°C. The agreement between the calculation and the measurement is satisfactory by applying this temperature offset. The existence of the offset means that either the measured crystal temperature read on the temperature controller or the poling periods specified by the manufacturer is not accurate. We verified that a plot of the theoretical values calculated with a poling period offset of $\Lambda - 0.02$ μm resulted also in the same plot as that with a temperature offset as shown in Fig. 3.

4 Threshold pump power

Figure 4 shows the measured threshold pump power, i.e. the input pump power at the oscillation threshold of the OPO, plotted as a function of signal and idler wavelengths. Note that the threshold pump power should be identical for the pair of the signal and idler waves which emit always simultaneously. In the wavelength range from 800 nm to 890 nm and from 1330 nm to 1600 nm for the signal and idler wavelength, respectively, the threshold pump power is kept as low as 0.4 W in average. The minimum measured value of the threshold pump power is 0.3 W. Outside of this low-threshold range, the threshold pump power increases rapidly,which is due to the decreasing reflectivity of the cavity mirrors for the resonant signal wave.

In order to verify whether the achieved threshold is close to the optimum value, we calculate the threshold pump power P_{th} according to the following equation derived from the steady-state threshold gain of a singly-resonant OPO with an optimally focused Gaussian beam [3]:

$$P_{\text{th}} = \frac{\epsilon_0 c n_s^2 \lambda_p \lambda_s \lambda_i}{4\pi^2 d_{\text{eff}}^2 L_c}(1 - R_s T_c). \tag{7}$$

Here, n_s denotes the refractive index of the OPO crystal at the signal wavelength, d_{eff} the effective nonlinear coefficient of the crystal, L_c the geometric length of the crystal, R_s the power reflectivity of the cavity mirrors (assumed the same for both mirrors) for the signal wave, and T_c the power transmission through the crystal for the signal wave. The terms λ_p, λ_s, λ_i denote the pump, signal, and idler wavelength to be fixed at 532 nm, 880 nm, and 1345 nm, respectively. The symbols ε_0 and c in (7) are the permittivity and the speed of light in free space, respectively.

For calculation, we used the data $d_{\text{eff}} = 16$ pm/V for a 5% MgO-doped PPLN based on the relation $d_{\text{eff}} = (2/\pi)d_{33}$ for the first-order quasi-phase matching with $d_{33} = 25$ pm/V measured for second-harmonic generation at 1064 nm [23].

For the mirror reflectivity, we use $R_s = 0.99$ from the assumption that the total mirror loss of 2% in the experiment is evenly distributed to both mirrors. The power transmission of the crystal T_c considers not only the absorption loss in the crystal but also the losses due to scattering and Fresnel reflections. The absorption loss is estimated from the linear absorption coefficient $\alpha = 0.003\ \mathrm{cm}^{-1}$ in the infrared (1064 nm) [20] according to the equation $T_c^a = \exp(-\alpha L_c)$ to be 0.988. The scattering and Fresnel loss at one anti-reflection coated facet of the crystal is estimated to be 0.2% so that, for the single-pass transmission, we have $T_c^b = 0.996$. By multiplying these two values of transmission, we get $T_c = T_c^a \cdot T_c^b = 0.984$. For the other parameters in (7), we use $n_s = 2.2$ and $L_c = 40$ mm.

As a result of calculation using the parameter values above, we obtain for the theoretical threshold pump power $P_{\mathrm{th}} = 0.52$ W, which is larger than the measured minimum threshold of 0.3 W. Consequently, we can conclude that, within the accuracy limit of the parameter estimation for calculation, the experimentally measured values in Fig. 4 can be regarded as the optimum for the given experimental parameters.

5 Output power and thermal effects

At the operation condition corresponding to each point in Fig. 4, we measured the output signal and idler power as a function of the pump power. To measure the output power at the signal and idler beams separately and simultaneously, two identical power meter detectors (LM-10, Coherent) are placed at each free-space output beam and their signals are recorded using a computer-controlled dual-channel readout instrument (LabMaster Ultima, Coherent). The sampling time of a single reading and the number of repetition for averaging were approximately 1 s and 10, respectively. At each single reading, the signal and idler power values are successively recorded within the sampling time. The pump power is determined from the set value of the pump laser which is calibrated to the measured values in front of the mode-matching lens (F1 in Fig. 1).

Figure 5 shows the measured OPO output power as a function of the input pump power for a poling period Λ of 7.2 μm at a crystal temperature of 40°C. The signal and idler wavelengths are measured to be 885.2 nm and 1333.3 nm, respectively. The OPO begins to oscillate already for a pump power near 0.3 W, and the signal and idler power increase with almost the same slope as the pump power is raised up to 1.3 W. For the pump power higher than 1.3 W, however, the signal power begins to decrease with the increasing pump power while the idler power seems to be saturated. The proportionality of the signal power to the idler power, which originates from the Manley–Rowe relation of the parametric

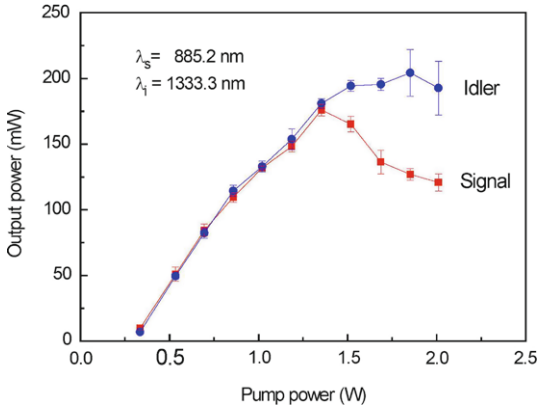

Fig. 5 Output power of the singly-resonant cw OPO at a signal and an idler wavelength of 885.2 nm and 1333.3 nm, respectively, as a function of the input pump power. The *square* and *circle symbols* indicate the measured power values of the signal and idler beams, respectively, which are successively measured within a time interval of approximately 1 s at each pump power. The error bars correspond to the standard deviations of the 10 repeated measurements at each pump power. The *lines* connect the *symbols* only for better visibility

interaction [24], is broken at high pump power, which indicates the existence of a power-dependent and wavelength-selective loss mechanism inside the OPO cavity. Thermal effects including lensing induced by power absorption inside the MgO-doped PPLN crystal can cause such a mechanism [15, 16]. Note that the influence of thermal effects on the resonant signal wave should be stronger than on the non-resonant idler wave of the singly-resonant OPO, which explains the asymmetric degradation of output power at the signal and idler beams.

The spectrum of the OPO output is measured and monitored by using a scanning confocal Fabry–Pérot interferometer (model FPI100, Toptica, FSR of 1 GHz) at the idler wavelength. The operation of single longitudinal mode is confirmed with a spectral linewidth of less than 5 MHz, which was the resolution limit of the used interferometer. We observed that the single-mode operation was maintained for the pump power range shown in Fig. 5, although the frequency stability was reduced as the pump power increased. A multimode operation at a high pump power as reported in [5, 15] is, however, not observed in this OPO.

Figure 6 shows the signal and idler power measured at a fixed pump power of 2 W as a function of wavelength. The plot of the corresponding threshold pump power is shown in Fig. 4. From the two figures, we observe that the correlation between the output power and the threshold pump power is strongly disturbed by the degradation of the output power at the high pump power. The degradation shows a periodic dependence on the wavelength and is not symmetric between the signal and idler beams as shown in Fig. 5. At several wavelengths, for example at the idler wavelength near 1400 nm, the OPO output power drops down to zero at

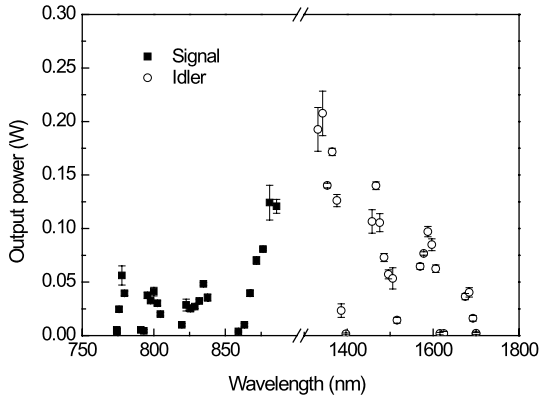

Fig. 6 Output power of the singly-resonant cw OPO as a function of output wavelength, measured at a pump power of 2 W

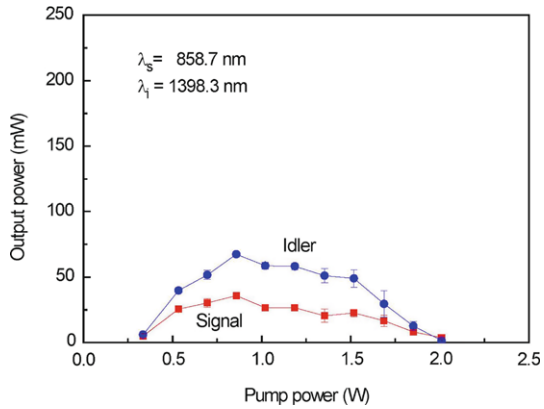

Fig. 7 Output power of the singly-resonant cw OPO at a signal and an idler wavelength of 858.7 nm and 1398.3 nm, respectively, as a function of the input pump power. The *square* and *circle* symbols indicate the measured power values of the signal and idler beams, respectively, which are successively measured within a time interval of approximately 1 s at each pump power. The error bars correspond to the standard deviations of the 10 repeated measurements at each pump power. The *lines* connect the *symbols* only for better visibility

a pump power of 2 W. The power characteristic at this operation condition is shown in Fig. 7, which is measured at the signal and idler wavelengths of 858.7 nm and 1398.3 nm, respectively, for a poling period Λ of 7.2 μm at a crystal temperature of 100°C.

In Fig. 7, the threshold pump power is below 0.4 W as similar to the condition in Fig. 5. That means that, according to (7), the cavity loss, the nonlinearity, and the cavity optimization at a low pump power are comparable between the two measurements. However, as the pump power increases, the slope efficiency in Fig. 7 is lower than in Fig. 5, and the degradation due to thermal effects is stronger so that the OPO stops to operate at a pump power of 2 W. Note that, for all the measurements shown in Figs. 5–7, the OPO is optimized for the minimum oscillation threshold and its alignment is not changed during the output power measurement at different pump power. From Fig. 6 and Fig. 3, we can

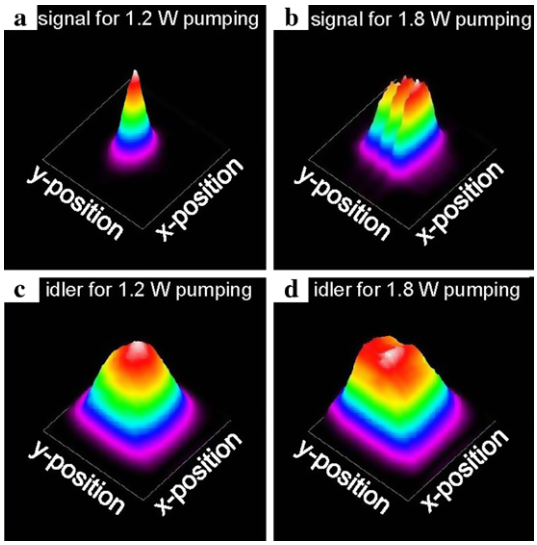

Fig. 8 Spatial power distribution of the output beams (beam profiles) of the singly-resonant cw OPO measured at the operation condition of Fig. 5. Pictures (**a**) and (**b**) are the signal beam profiles at a pump power of 1.2 W and 1.8 W, respectively. Pictures (**c**) and (**d**) are the idler beam profiles at a pump power of 1.2 W and 1.8 W, respectively

identify that the output power degradation due to thermal effects becomes stronger as the crystal temperature increases. Such a correlation between the thermal lensing and the crystal temperature is reported also for a green-pumped OPO based on MgO-doped stoichiometric PPLT [4]. The magnitude of thermal lensing seems to be stronger for a MgO-doped PPLN crystal than that for a MgO-doped stoichiometric PPLT crystal. For a quantitative discussion, however, a precise measurement of the crystal absorption coefficient as a function of temperature and input power for both the crystals is required.

Finally, we measured the spatial power distribution of the output beams (beam profiles) to verify that thermal lensing is a dominant effect degrading the output power at high pump power. Figure 8 shows the beam profiles measured at the operation condition of Fig. 5 using a scanning-slit beam profiler (BP104-IR, Thorlabs). Figures 8(a) and 8(b) are the signal beam profiles at a pump power of 1.2 W and 1.8 W, respectively. The signal beam profile in Fig. 8(a) is close to a Gaussian mode as expected from the cavity resonance. At a high pump power in Fig. 8(b), however, we clearly see a severe distortion of the spatial mode, which can be explained by excitation of higher-order transversal cavity modes due to thermal lensing. Such a degradation of the spatial mode due to thermal lensing in a MgO-doped PPLN crystal is reported also for the infrared-pumped cw OPOs [15, 16], but it obviously occurs at lower pump power for the green-pumped cw OPOs [5]. The distortion of the spatial mode degrades the spatial-mode matching and, consequently, the conversion efficiency of the OPO. This behavior is also confirmed for the idler beam profiles in Figs. 8(c) and 8(d), but the effect is

relatively weak compared to that of the signal beam. Note that the difference between the signal and idler beams at low pump power is because we use a common collimating lens (F2 in Fig. 1) for the two beams with different wavelengths and divergence.

6 Continuous frequency tuning

Continuous frequency tuning is one of the important features that make the singly-resonant cw OPO useful for a variety of applications. In order to verify the single resonance of the low-threshold linear-cavity OPO, we measured the frequency range of the continuous tuning by scanning the cavity length using the PZT behind one cavity mirror (see in Fig. 1). For an ideal singly-resonant OPO without any frequency-selective element such as an etalon inside the cavity, we expect that the maximum frequency range of the continuous tuning is limited by the FSR of the OPO cavity. In reality, however, there exist a spurious gain modulation due to ambient fluctuations and also a weak intra-cavity etalon by residual reflectance of the components at the non-resonant wavelength, which reduce the continuous-tuning range by inducing a mode hop [15]. Therefore, the measurement of the continuous-tuning range as a ratio to the FSR provides information upon the quality of the single resonance of the OPO cavity.

We measured the continuous tuning range of the OPO using a fiber etalon depicted in Part B of Fig. 1. We coupled the idler beam to a polarization-maintaining (PM) single-mode fiber (SMF) with a geometrical length of 2 m and the transmitted output through the fiber is monitored using an InGaAs photodiode. As the facets of the PM-SMF are polished plane-parallel to each other and are not anti-reflection coated, the PM-SMF itself builds a low-finesse etalon. With the refractive index of 1.5 for a silica fiber in the infrared, we estimate the FSR of this fiber etalon to be 50 MHz. When the frequency of the idler output from the OPO is linearly varied by scanning the length of the OPO cavity, we expect to observe an interference fringe in the transmission of the fiber etalon whose maximum is repeated for a tuning of 50 MHz. Measurement of a smooth interference fringe without discontinuity proves a continuous frequency tuning of the OPO and its tuning range can be determined from the number of the maxima within the continuous-tuning range multiplied by the FSR of the fiber etalon [25].

Figure 9 shows a measurement result of the continuous frequency tuning. From the smooth interference fringe between the two mode hops in the idler transmission through the fiber etalon, the continuous frequency tuning is proved. The frequency range of the continuous tuning is determined to be 800 MHz, which is close to 90% of the FSR of the OPO cavity of 900 MHz. Compared to the result of 95% for a four-mirror traveling-wave cavity OPO in [25], this result of 90% seems acceptable for a singly-resonant OPO with a two-mirror standing-wave cavity.

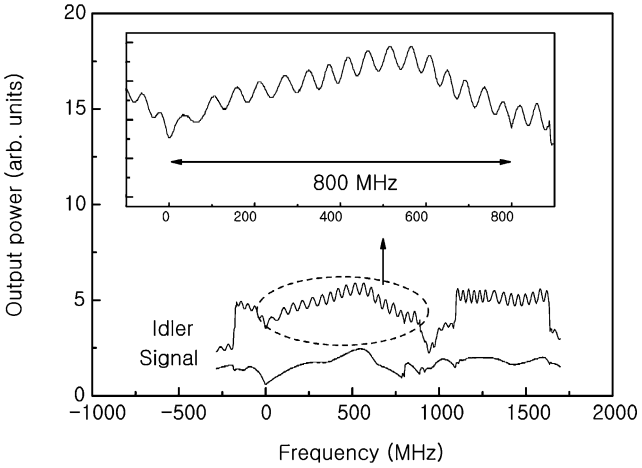

Fig. 9 Idler power transmitted through the fiber etalon as a function of tuning frequency that is scaled based on the free spectral range (50 MHz) of the 2-m long fiber etalon. The signal output power without the interference fringe is also shown for comparison. The *inset* shows the fringe part of continuous frequency tuning between two mode hops whose range is determined to be 800 MHz, corresponding to 90% of the FSR of the OPO cavity

7 Summary

We presented a singly-resonant linear-cavity cw OPO based on MgO-doped PPLN optimized for a low oscillation threshold. Pumped at 532 nm, the OPO operates at a threshold pump power of below 0.5 W in the wavelength tuning range from 800 to 890 nm and from 1330 to 1600 nm for the signal and idler, respectively. The measured minimum value of the threshold pump power was as low as 0.3 W while the theoretical calculation based on the estimated experimental parameters resulted in a value of 0.52 W, indicating a successful optimization of the experimental setup.

We described the optimization method of the OPO in detail. We used a tunable diode laser at a wavelength close to a signal wavelength to monitor the alignment and the confocal parameter of the OPO cavity. The cavity length and the focusing of the pump beam is adjusted to optimize the spatial match of the pump beam to the cavity mode. When the OPO starts to operate after the initial optimization, we maximized the output power at a pump power slightly above the threshold to minimize the oscillation threshold.

The maximum output power at a pump power of 2 W was approximately 100 mW and 200 mW at the signal and idler wavelength of 885 nm and 1333 nm, respectively. However, the performance of output power was limited by thermal effects in the crystal. We measured a strong degradation of the power and spatial-mode quality of the output beams as

the pump power increases, which indicates a strong thermal lensing. In addition, we observed that the performance degradation due to thermal effects seems to be dependent on the crystal temperature.

Finally, we demonstrated a continuous frequency tuning of the OPO by using a fiber etalon. The measured frequency range of the continuous tuning was 800 MHz corresponding to approximately 90% of the FSR of the OPO cavity.

References

1. R.G. Smith, J.E. Geusic, H.J. Levinstein, J.J. Rubin, S. Singh, L.G. Van Uitert, Appl. Phys. Lett. **12**, 308 (1968)
2. L.E. Myers, R.C. Eckardt, M.M. Fejer, R.L. Byer, W.R. Bosenberg, J.W. Pierce, J. Opt. Soc. Am. B **12**, 2102 (1995)
3. R.L. Sutherland, *Handbook of Nonlinear Optics*, 2nd edn. (Marcel Dekker, New York, 2003), Chap. 3
4. G.K. Samanta, G.R. Fayaz, Z. Sun, M. Ebrahim-Zadeh, Opt. Lett. **32**, 2623 (2007)
5. S. Zaske, D.-H. Lee, C. Becher, Appl. Phys. B **98**, 729 (2010)
6. J.E. Bjorkholm, Appl. Phys. Lett. **13**, 399 (1968)
7. S.T. Yang, R.C. Eckardt, R.L. Byer, Opt. Lett. **18**, 971 (1993)
8. S.T. Yang, R.C. Eckardt, R.L. Byer, Opt. Lett. **19**, 475 (1994)
9. W.R. Bosenberg, A. Drobshoff, J.I. Alexander, L.E. Myers, R.L. Byer, Opt. Lett. **21**, 713 (1996)
10. W.R. Bosenberg, A. Drobshoff, J.I. Alexander, L.E. Myers, R.L. Byer, Opt. Lett. **21**, 1336 (1996)
11. R.G. Batchko, D.R. Weise, T. Plettner, G.D. Miller, M.M. Fejer, R.L. Byer, Opt. Lett. **23**, 168 (1998)
12. A.V. Okishev, J.D. Zuegel, Opt. Express **14**, 12169 (2006)
13. T.-H. My, O. Robin, O. Mhibik, C. Drag, F. Bretenaker, Opt. Express **17**, 5912 (2009)
14. P. Gross, I.D. Lindsay, C.J. Lee, M. Nittmann, T. Bauer, J. Bartschke, U. Warring, A. Fischer, A. Kellerbauer, K.-J. Boller, Opt. Lett. **35**, 820 (2010)
15. M. Vainio, J. Peltola, S. Persijn, F.J.M. Harren, L. Halonen, Appl. Phys. B **94**, 411 (2009)
16. A. Henderson, R. Stafford, Appl. Phys. B **85**, 181 (2006)
17. H. Kolgenik, T. Li, Appl. Opt. **5**, 1550 (1966)
18. G.D. Boyd, D.A. Kleinman, J. Appl. Phys. **39**, 3597 (1968)
19. D.-H. Lee, S.K. Kim, S.-N. Park, H.S. Park, J.Y. Lee, S.K. Choi, Appl. Opt. **48**, 37 (2009)
20. V.G. Dmitriev, G.G. Gurzadyan, D.N. Nikogosyan, *Handbook of Nonlinear Optics*, 3rd edn. (Springer, Berlin, 1999)
21. A.E. Siegman, *Lasers* (University Science Books, Mill Valley, 1986), Chap. 17
22. O. Gayer, Z. Sacks, E. Galun, A. Arie, Appl. Phys. B **91**, 343 (2008)
23. I. Shoji, T. Kondo, A. Kitamoto, M. Shirane, R. Ito, J. Opt. Soc. Am. B **14**, 2268 (1997)
24. W.H. Louisell, A. Yariv, A.E. Siegman, Phys. Rev. **124**, 1646 (1961)
25. M.E. Klein, D.-H. Lee, J.-P. Meyn, K.-J. Boller, R. Wallenstein, Opt. Lett. **24**, 1142 (1999)